Supporting Information

Toroidal ferroelectric cobalt-doped barium titanates as efficient energy conversion materials for solar cells and photocatalysis

Murali Balu[a], Duraisamy Kumaresan[a,b,*] R. Krishna Prasad[a,b], Subhash Kalidindi[c]

[a] Solar Energy and Optoelectronics Research Laboratory, COE-AMGT, Amrita School of Engineering, Coimbatore 641112, Amrita Vishwa Vidyapeetham, India

[b] Department of Chemical Engineering and Materials Science, Amrita School of Engineering, Coimbatore, Amrita Vishwa Vidyapeetham, India

[c] Department of Chemical and Biological Engineering, Tufts University, Medford, Massachusetts 02155, United States.

* E-mail: k_duraisamy@cb.amrita.edu, *Tel: +91-422-2685000.*

Materials

All experiments were performed using HPLC-grade solvents without further purification. Anatase titanium (IV) oxide nanopowder (~ 25 nm size particles) (99.7%), cobalt (II) chloride hexahydrate, NaOH pellets, hydrochloric acid (HCl, 35.5%), LiI, $H_2PtCl_6 \cdot 6H_2O$, iodine, 4-tert-butyl pyridine (96%), glacial acetic acid, $Ba(OH)_2 \cdot 8H_2O$ (≥98%) were purchased from Sigma-Aldrich (India). Fluorine-doped tin oxide (FTO) conducting glass slides (2.2 mm thickness) were purchased from Greatcell Solar (Dyesol), Australia. Photosensitizer N719 [cis-diisothiocyanato-bis(2,2'-bipyridyl-4,4'-dicarboxylato) ruthenium (II) bis(tetrabutylammonium)] dye and Surlyn® ionomer film were procured from Dyenamo, Sweden.

Methods

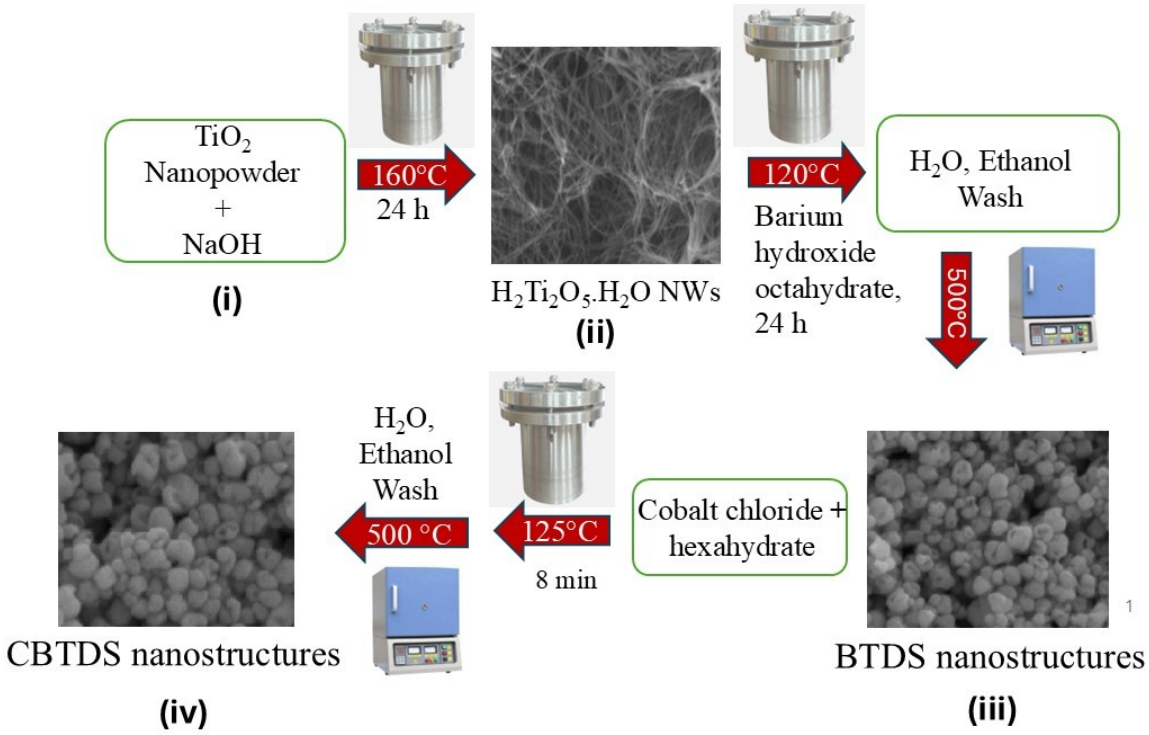

$$TiO_2 + 2\ NaOH + H_2O \rightarrow Na_2Ti_2O_5.H_2O \quad \textbf{(i)}$$

$$Na_2Ti_2O_5.H_2O + 6\ HCl \rightarrow H_2Ti_2O_5.H_2O + 2\ NaCl + 3\ H_2O \quad \textbf{(ii)}$$

$$H_2Ti_2O_5.H_2O + 3\ Ba(OH)_2.8H_2O \rightarrow BaTiO_3 + 2\ Ba(OH)_2 + 6\ H_2O \quad \textbf{(iii)}$$

$$BaTiO_3 + 3\ CoCl_2.6H_2O \rightarrow 3\ CoBaTiO_3 + 6\ HCl + 13\ H_2O \quad \textbf{(iv)}$$

Scheme S1: Chemical reactions for the formation of BDTS and CBDTS nanostructures.

Preparation of BTDS light-scattering layer paste

To make the BTDS scattering layer paste, 1 g BTDS dry nanopowder, 0.3 g ethyl cellulose, 2 ml terpinol, 1 ml acetic acid, and 10 ml ethanol were stirred with a magnetic stirrer in an Erlenmeyer flask for 45 min. The resultant mixture was then ultrasonicated for 1 h to produce a white sol. After that, this mixture was magnetically stirred for 24 h at 300 rpm to obtain a uniform white paste.

Preparation of CBTDS light-scattering layer paste

To prepare the scattering layer paste of CBTDS, 1 g CBTDS nanopowder, 0.3 g ethyl cellulose, 2 ml terpinol, 1 ml glacial acetic acid, and 10 ml absolute ethyl alcohol were added sequentially to obtain a pale green mixture. The subsequent mixture was then ultrasonicated for 1 h to produce a smooth, pale green sol/dispersion. This green colloidal sol was magnetically stirred for 24 h at 300 rpm to form a homogeneous pale green paste.

Dye desorption study

The TNP + BTDS and TNP + CBTDS bilayer photoanodes coated with N719 dye were individually immersed in a 1 M aqueous sodium hydroxide solution for 30 min for the dye to desorb into the alkaline solution completely. Then, the UV-visible absorption spectra of N719 dye desorbed solutions were recorded to estimate the dye concentrations. The desorbed dye concentration data were used to quantify the dye uptake value of each bilayer photoanode.

Characterization instruments

The crystal structure and phase of HTNWs, BTDS, and CBTDS were determined using the X-ray diffractometer (Rigaku Ultima IV), with a scan step size of 0.02/s irradiated with the characteristic Cu-Kα radiation wavelength (λ=0.154 nm). SIGMA HV–Carl Zeiss field emission scanning electron microscopy (FESEM) was used to investigate the surface morphological features of as-prepared HTNWs, BTDS, and CBTDS nanostructures. Brunauer-Emmett-Teller (BET) specific surface area and Barrett-Joyner-Halenda (BJH) methods were employed for the average pore size and pore volume distribution analysis of BTDS and CBTDS nanostructures performed with nitrogen adsorption/desorption isotherms recorded by using a Quantachrome ASiQwin™ instrument. The absorbance and diffuse reflectance spectra of single-layer BTDS and CBTDS photoelectrode were recorded using a UV-visible-NIR (Shimadzu 2600) spectrophotometer in 200-1400 nm spectral regions. Chemical analysis of

the samples for elemental composition and chemical state of elements present at the surfaces was performed by the Kratos Analytical, AXIS Supra, X-ray photoelectron spectrometer (XPS). The photovoltaic outputs of DSSCs were obtained from their current density-voltage (J-V) recorded by using a Keithley 2400 source meter and under simulated solar irradiation of AM1.5 G conditions delivered by a Newport solar simulator. A square mask (0.16 cm^2) matching the active area of DSSCs was employed to control the illumination area during the J-V measurements. The incident photon to charge carrier efficiency (IPCE) spectra of samples were obtained using a Newport-Oriel instruments (TLS-300XU) setup equipped with a Cornerstone monochromator, a 300-watt xenon arc source, and a calibrated silicon photodiode. The electrochemical impedance spectroscopy (EIS) measurements were performed using a CH Instruments electrochemical analyzer (Model 604E), USA. The EIS data were recorded using an electrochemical workstation (CH Instruments) under the applied frequency range from 100 kHz to 0.1 Hz at a bias potential range from -0.5 to -0.8 V with an amplitude of 10 mV. All bilayer photoelectrode-based DSSCs impedance spectra were fitted using an equivalent circuit model available with the Z-view software.

S1: X-ray diffraction pattern of as-synthesized $H_2Ti_2O_5.H_2O$ nanowires.

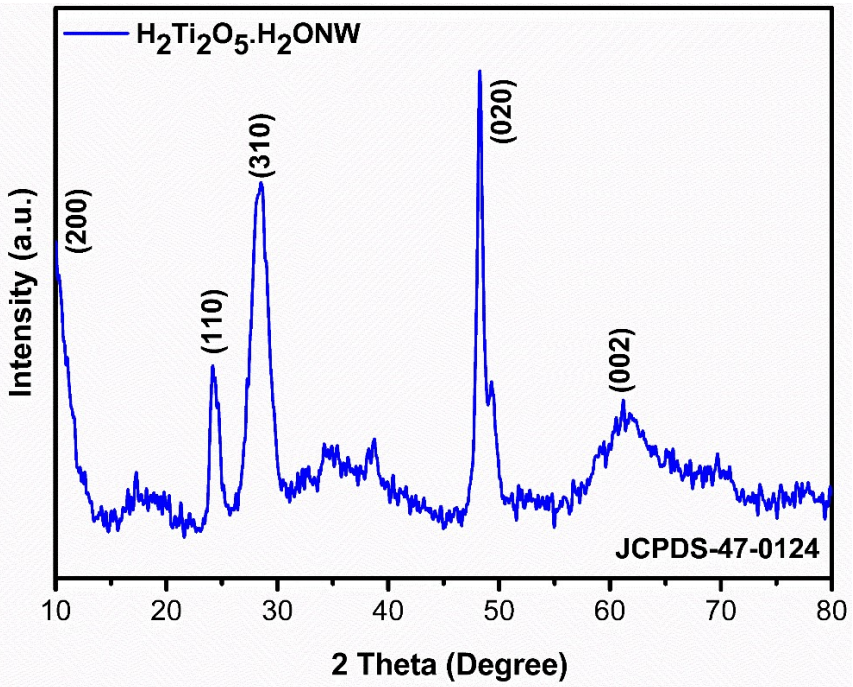

S2: Table of crystallite size and particle size distribution of BTDS and CBTDS nanostructures.

Sample	XRD estimated crystallite size (nm)	TEM measured crystallite size (nm)
BTDS	33.9	34.0
CBTDS	42.0	42.1

S3: High and low magnification FESEM images of the $H_2Ti_2O_5.H_2O$ nanowires.

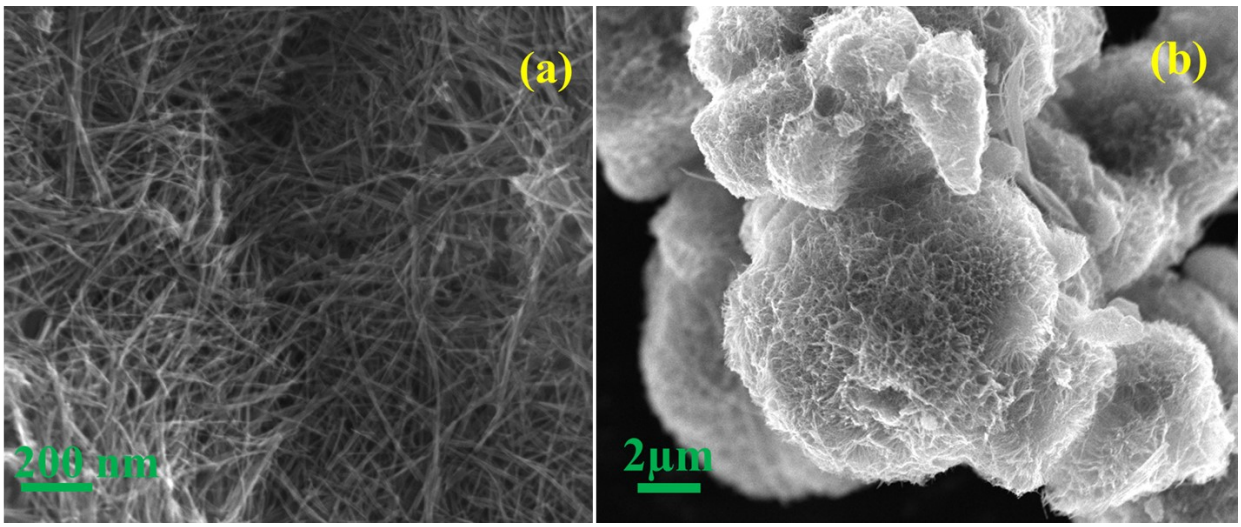

S4: The images of (a) the SEM elemental mapping of BTDS nanostructures and (b) the EDS spectrum.

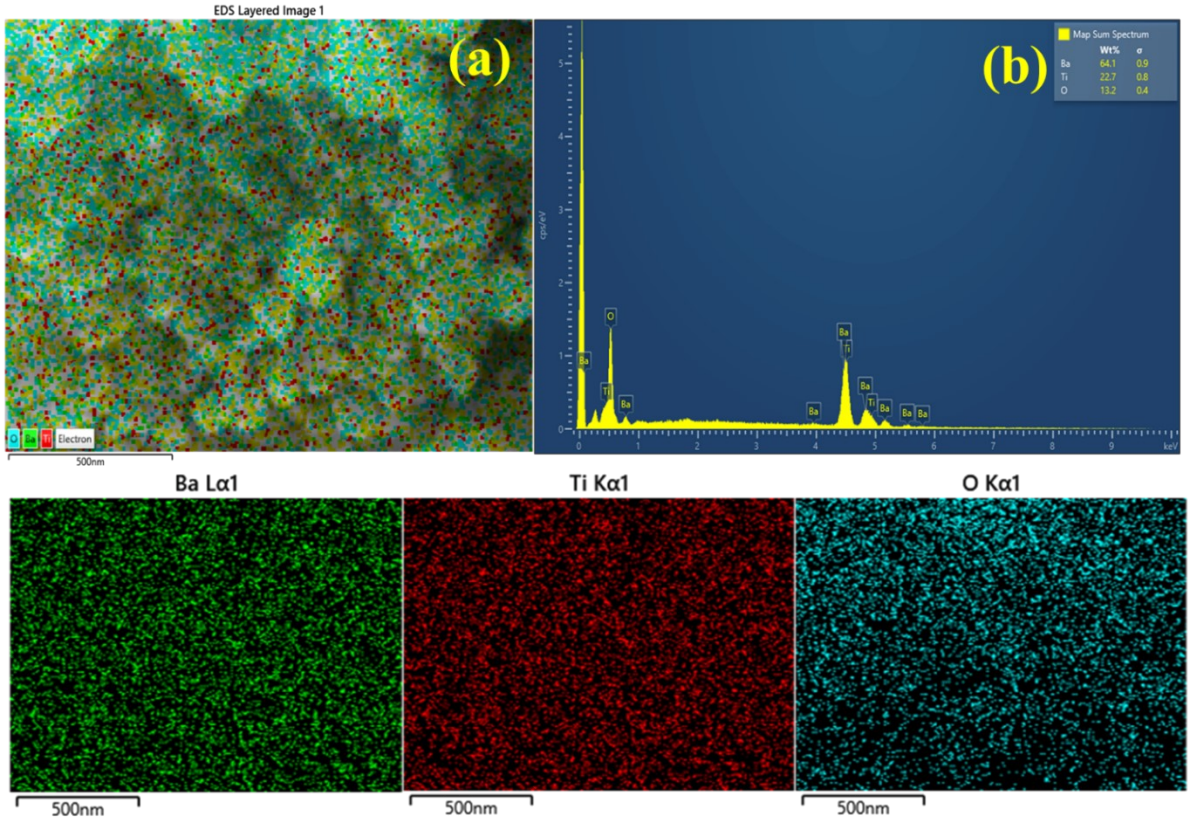

S5: The images of (a) the SEM elemental mapping of CBTDS nanostructures and (b) the EDS spectrum.

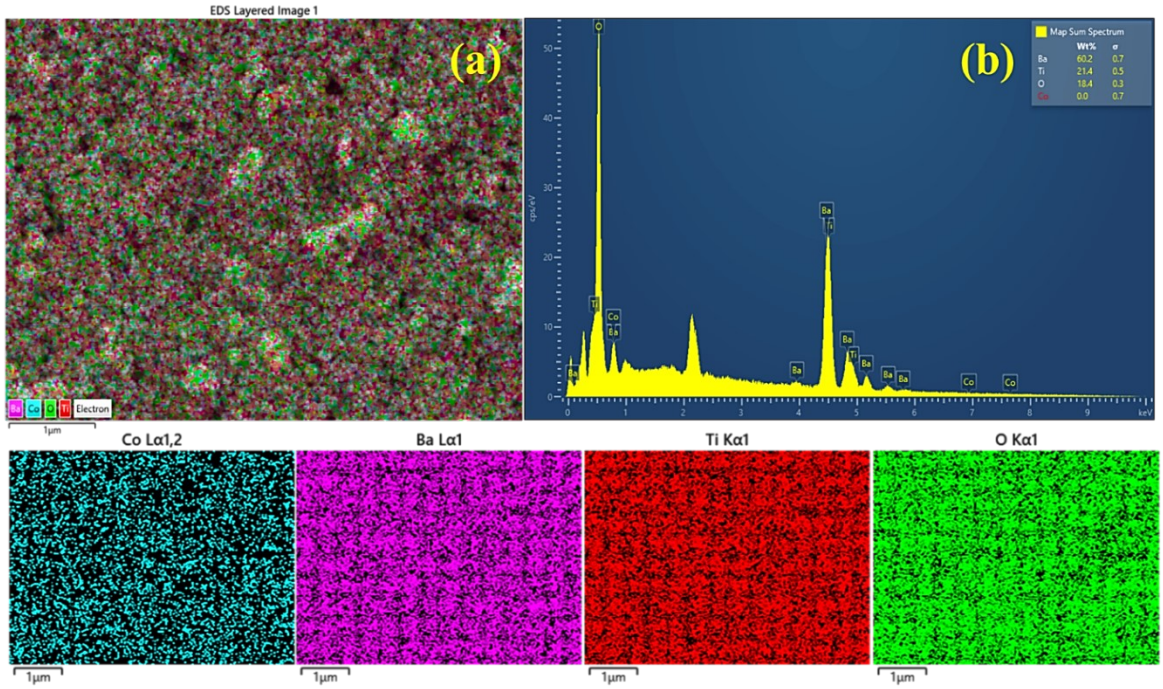

Table S5: Elemental composition of CBTDS obtained from SEM EDS analysis.

Element	Wt.%	σ
Ba	**60.2**	**0.7**
Ti	**21.4**	**0.5**
O	**18.4**	**0.3**
Co	**0.0**	**0.7**

S6: The HRTEM-EDS spectra of (a) BTDS and (b) CBTDS.

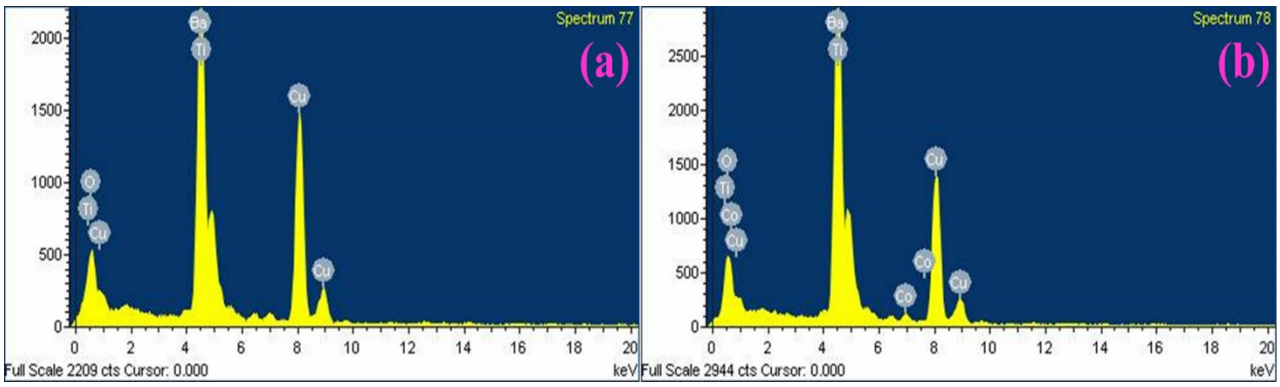

S7: Table of BET and BJH data of the as-prepared nanostructures; the percentage porosity was estimated from P=Pv/[(1/ρ) + Pv] in percent value, where (1/ρ) represents the inverse density of BTDS and CBTDS.

Sample	BET Surface Area [m^2/g]	Pore Volume [cc/g]	Pore size [nm]	Pore diameter [nm]	Porosity [%]
BTDS	25.843	0.069	26.44	3.098	16.97
CBTDS	20.978	0.047	27.32	3.129	11.65

S8: (a) UV-visible-NIR absorption spectra, (b) Tauc plots, and (c) Schematic representation of toroidal geometry with Gorbatsevich and Kopaev-type toroidal polarization in the BTDS and CBTDS nanostructures.

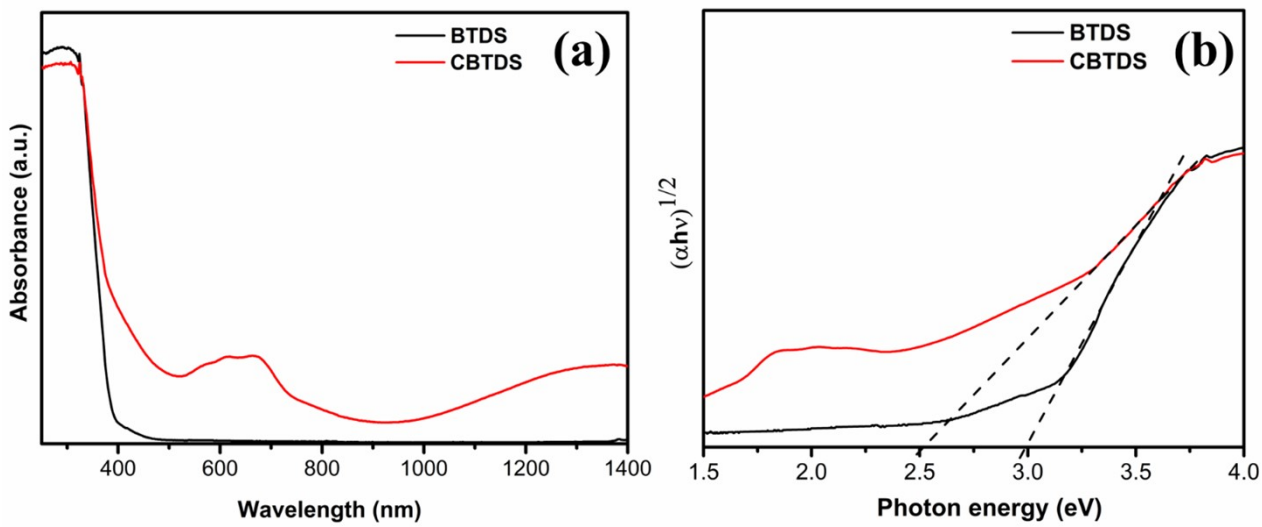

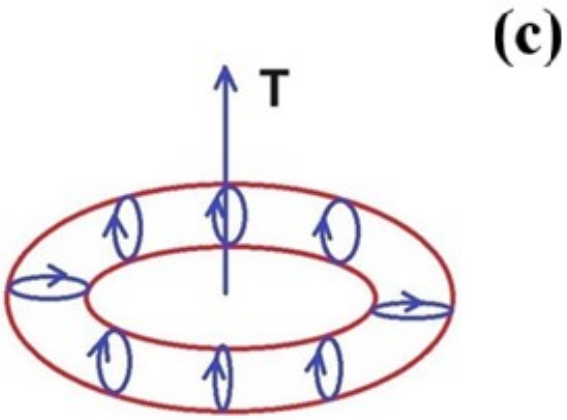

S9: Wide scan XPS survey spectra of BTDS and CBTDS nanostructures.

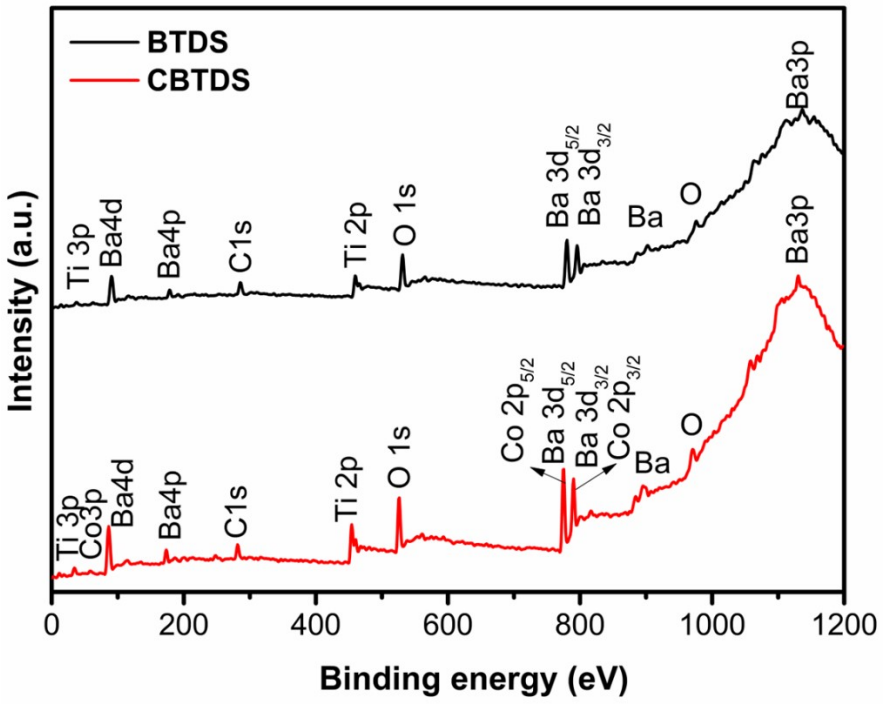

S10: Absorption spectra of N719 dye desorbed from the TNP+BTDS and TNP+CBTDS bilayer photoanodes

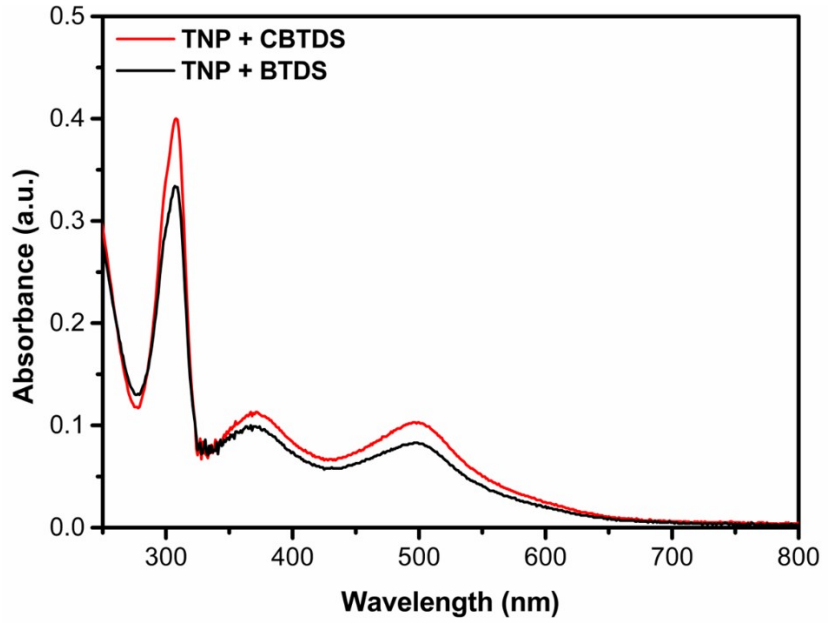

S11. Photovoltaic J-V curves of monolayer CBTDS and bilayer TNP + CBTDS nanostructures without N719 dye as a photoactive layer of DSSC photoelectrode.

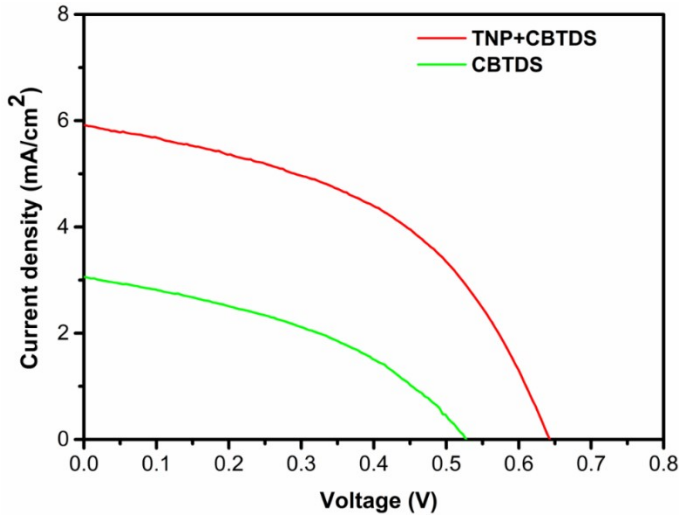

S12: EIS parameters derived traces of (a) Chemical capacitance, (b) Diffusion coefficient, (c) Diffusion length, and (d) Charge collection efficiency of bilayer TNP + BTDS and TNP + CBTDS photoelectrodes at various applied potentials from -0.4V to -0.8V.